

Electronic Supplementary Information

Cocrystallization in VB₉ gels to construct stoichiometry-controlled isostructural materials

Junjie Bao ^{ab}, Zaiyong Zhang ^b, Zhicheng Yan ^{ab}, Jian-Rong Wang ^{*b}, and Xuefeng

Mei ^{*b}

^a *Nano Science and Technology Institute, University of Science and Technology of China, Suzhou, Jiangsu 215123, China.*

^b *Pharmaceutical Analytical & Solid-State Chemistry Research Center, Shanghai Institute of Materia Medica, Chinese Academy of Sciences, Shanghai 201203, China.*

EXPERIMENTAL SECTION

Materials. Acridine (**acr**), 4-chlorophenol (**clp**), 4-bromophenol (**brp**), or 4-iodophenol (**ip**), vitamins C, and B₉ were obtained from J&K Chemical Ltd, with greater than 99% purity. All analytical grade solvents were purchased from Sinopharm Chemical Reagent Co., Ltd and used without further purification.

Gel formation (Vial inversion test). Method A: 4 mg of VB₉ was dissolved in 1 mL methanol and heated up until it resulted in a clear solution. After cooling down to room temperature the gel was formed within minutes. Method B: 6 mg of VB₉ was dissolved in 1 mL dimethyl sulfoxide / nitromethane (2:8) and heated up until it resulted in a clear solution. After cooling down to room temperature the gel was formed within minutes.

Preparation of (acr)·(clp). 35.8 mg (0.2 mmol) **acr** and 25.7 mg (0.2 mmol) **clp** were dissolved in 1 mL methanol by heating, respectively. The addition of 4 mg of VB₉ and cooling down to room temperature resulted in the immediate formation of gels, and then kept in 4 °C. Crystals grew within a few days. The gels are then dissolved by addition of 10 μL Et₃N. The orange platy crystals recovered by filtration.

Preparation of (acr)₂·(clp). 35.8 mg (0.2 mmol) **acr** and 12.8 mg (0.1 mmol) **clp** were dissolved in 1 mL methanol by heating, respectively. The addition of 4 mg of VB₉ and cooling down to room temperature resulted in the immediate formation of gels, and then kept in 4 °C. Crystals grew within a few days. The gels are then dissolved by addition of 10 μL Et₃N. The pale blue columnar crystals recovered by filtration.

Preparation of (acr)·(brp). 35.8 mg (0.2 mmol) **acr** and 34.6 mg (0.2 mmol) **brp** were dissolved in 1 mL methanol by heating, respectively. The addition of 4 mg of VB₉ and cooling down to room temperature resulted in the immediate formation of gels, and then kept in 4 °C. Crystals grew within a few days. The gels are then

dissolved by addition of 10 μL Et_3N . The colorless column-like crystals recovered by filtration.

Preparation of $(\text{acr})_2 \cdot (\text{brp})$. 35.8 mg (0.2 mmol) **acr** and 17.3 mg (0.1 mmol) **brp** were dissolved in 1 mL methanol by heating, respectively. The addition of 4 mg of VB_9 and cooling down to room temperature resulted in the immediate formation of gels, and then kept in 4 $^\circ\text{C}$. Crystals grew within a few days. The gels are then dissolved by addition of 10 μL Et_3N . The orange needle-like crystals recovered by filtration.

Preparation of $(\text{acr}) \cdot (\text{ip})$. 35.8 mg (0.2 mmol) **acr** and 44.0 mg (0.2 mmol) **ip** were dissolved in 1 mL methanol by heating, respectively. The addition of 4 mg of VB_9 and cooling down to room temperature resulted in the immediate formation of gels, and then kept in 4 $^\circ\text{C}$. Crystals grew within a few days. The gels are then dissolved by addition of 10 μL Et_3N . The colorless column-like crystals recovered by filtration.

Preparation of $(\text{acr})_2 \cdot (\text{ip})$. 35.8 mg (0.2 mmol) **acr** and 22.0 mg (0.1 mmol) **ip** were dissolved in 1 mL methanol by heating, respectively. The addition of 4 mg of VB_9 and cooling down to room temperature resulted in the immediate formation of gels, and then kept in 4 $^\circ\text{C}$. Crystals grew within a few days. The gels are then dissolved by addition of 10 μL Et_3N . The orange needle-like crystals recovered by filtration.

Thermogravimetric analysis (TGA). Thermogravimetric analysis was carried out in Netzsch TG 209 F3 equipment, using dry air with a nitrogen gas flow of 20 mL/min and a scan rate of 10 $^\circ\text{C}/\text{min}$.

Differential scanning calorimetry (DSC). Differential scanning calorimetry (DSC) was performed with a PerkinElmer DSC 8500 instrument under nitrogen gas flow of 20 mL/min purge. Samples weighting 3–5 mg were heated in standard aluminium pans at scan rates from 5 to 10 $^\circ\text{C}/\text{min}$. Two-point calibration using indium and tin was carried out to check the temperature axis and heat flow of the equipment.

Powder X-ray diffraction (PXRD). PXRD patterns were obtained using a Bruker D8 Advance X-ray diffractometer (Cu K α radiation). The voltage and current applied were 40 kV and 40 mA respectively. Samples were measured in reflection mode in the 2 θ range 3–40° with a scan speed of 1.2 °/min (step size 0.025°, step time 1.0 s) using a LynxEye detector. Data were imaged and integrated with RINT Rapid, and the peaks are analysed with Jade 6.0 software from Rigaku. Calibration of the instrument was performed using Corindon (Bruker AXS Korundprobe) standard.

Single crystal X-ray diffraction. Single crystals were performed on a Bruker Apex II CCD diffractometer using Mo K α radiation ($\lambda = 0.71073$ Å). The structures were solved by direct methods and refined with full-matrix least-squares difference Fourier analysis using SHELX-97 software. All non-hydrogen atoms were refined with anisotropic displacement parameters, and all hydrogen atoms were placed in calculated positions and refined with a riding model. Data were corrected for the effects of absorption using SADABS.

Fourier transform Infrared (FT-IR). Fourier transform Infrared (FT-IR) spectra were collected by a Nicolet-Magna FT-IR 750 spectrometer in the range of 4000 to 400 cm⁻¹ with a resolution of 4 cm⁻¹ at ambient conditions.

Molecular electrostatic potential (MEP) calculations. The MEPs presented in this work were computed using the CASTEP Software.^{S1} All the energy calculations were based on density-functional theory (DFT) in the generalized gradient approximation (GGA), as implemented in the CASTEP code. The optimized ultrasoft pseudopotentials for plane wave energy cutoff was 300 eV, and a Brillouin zone sampling of (3 \times 3 \times 1). All atomic position were relaxed until the maximal force on each atom was smaller than 0.01 eV/Å. MEP topographical analysis were performed. MEP at any point with the position vector \mathbf{r} can be calculated using the equation,

$$V(\mathbf{r}) = \sum_A^N \frac{Z_A}{|\mathbf{r} - \mathbf{R}_A|} - \int \frac{\rho(\mathbf{r}')d^3\mathbf{r}'}{|\mathbf{r} - \mathbf{r}'|} \quad (1)$$

where Z_A is the nuclear charge of atom A with radius vector RA . $\rho(r')$ is the electron density of the molecule and r' is a dummy integration variable.^{S2,S3} $V(r)$ is strongly dependent on the local charges around point r , the positive charges on the neighboring nuclei, and the electron density in closer vicinity of point r . The local most positive $V(r)$ was identified as $V_{s,max}$.

References

- S1. Payne, M. C.; Allan, D. C.; Arias, T. A.; Johannopoulos, J. D. *Rev. Mod. Phys.* 1992, **64**, 1045.
- S2. Gadre, S. R.; Shirsat, R. N. *Electrostatics of Atoms and Molecules*; Universities Press: Hyderabad, India, 2000.
- S3. Politzer, P.; Truhlar, D. G. *Chemical Applications of Atomic and Molecular Electrostatic Potentials*; Plenum Press: New York, 1981.

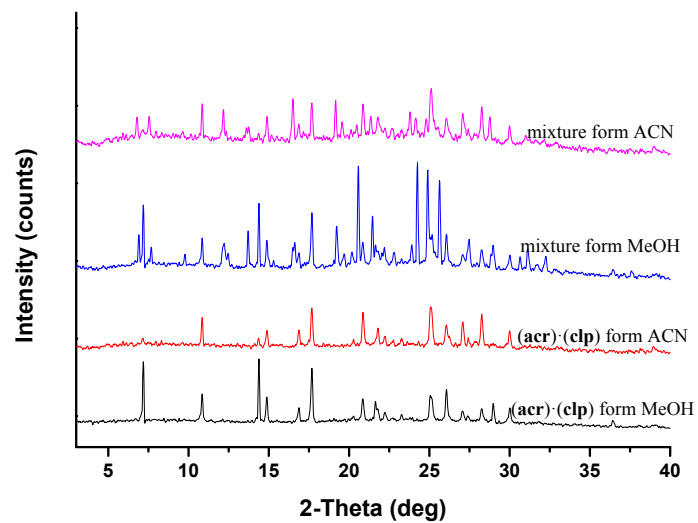


Fig. S1 PXR D patterns of solids form different solvents

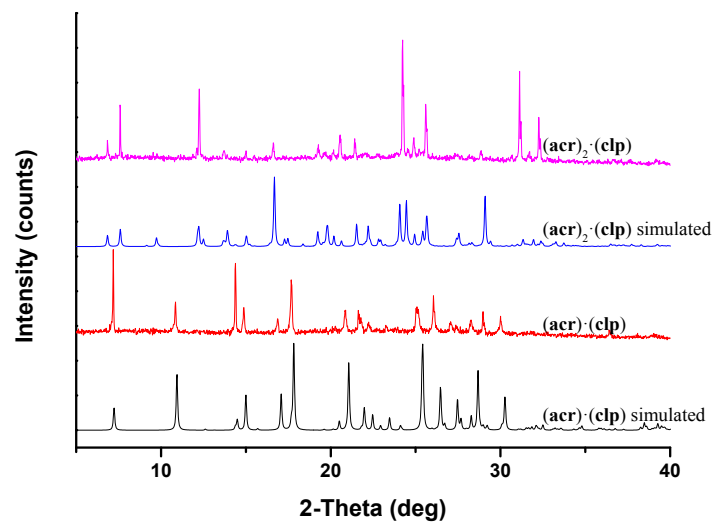


Fig. S2 PXR D patterns of cocrystals $(acr) \cdot (clp)$ and $(acr)_2 \cdot (clp)$.

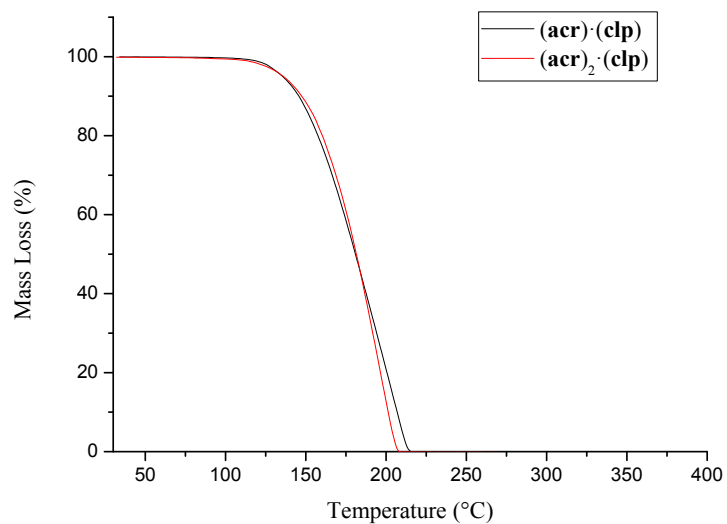


Fig. S3 TGA thermograms of cocrystals **(acr)·(clp)** and **(acr)₂·(clp)**.

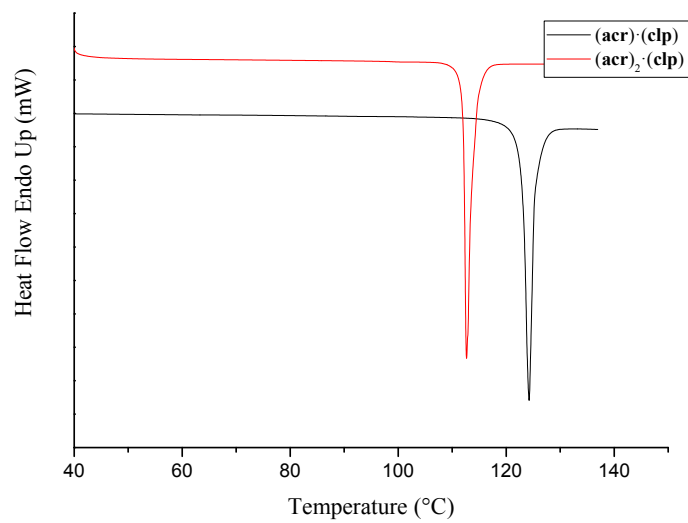


Fig. S4 DSC thermograms of cocrystals **(acr)·(clp)** and **(acr)₂·(clp)**.

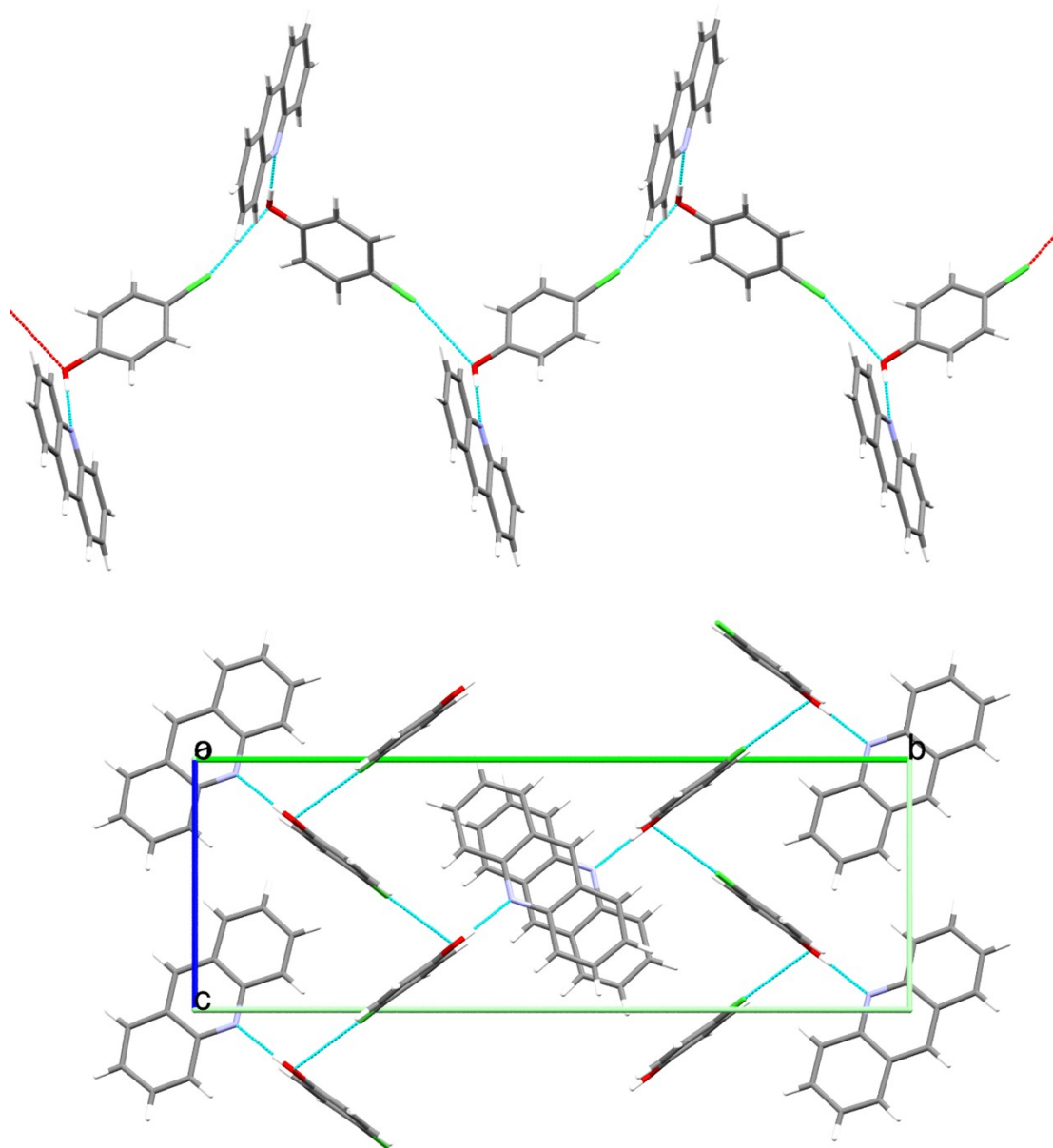


Fig. S5 Crystal structure of (acr)·(clp).

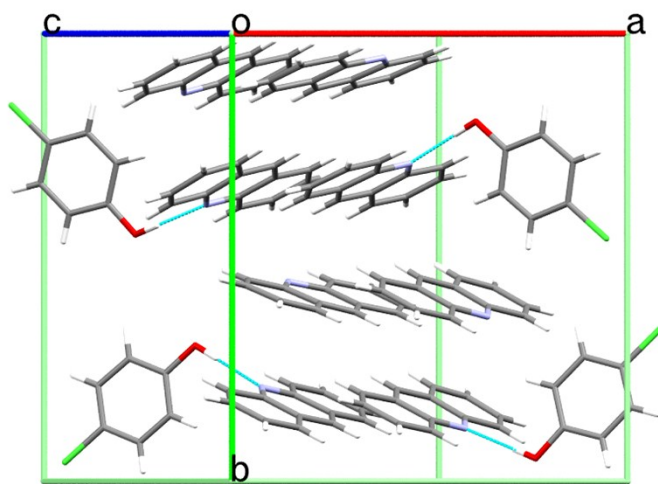
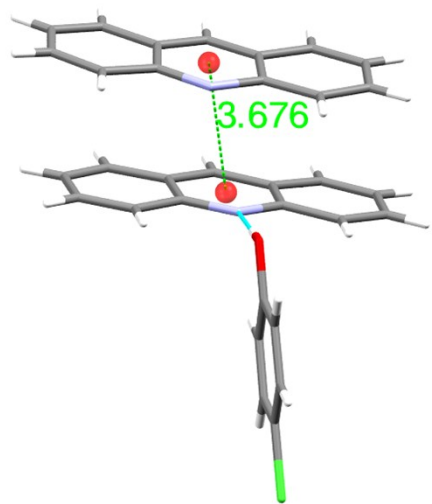


Fig. S6 Crystal structure of $(acr)_2 \cdot (clp)$.

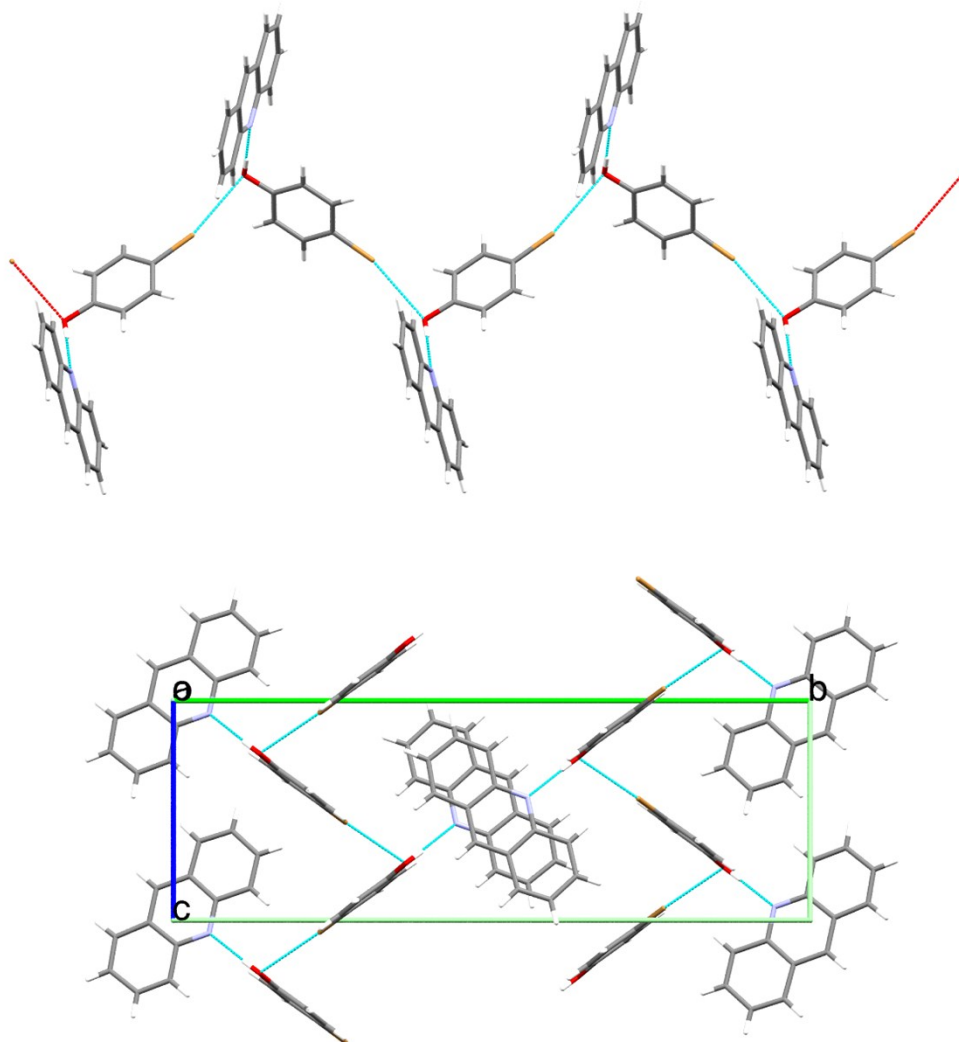


Fig. S7 Crystal structure of (acr)·(brp).

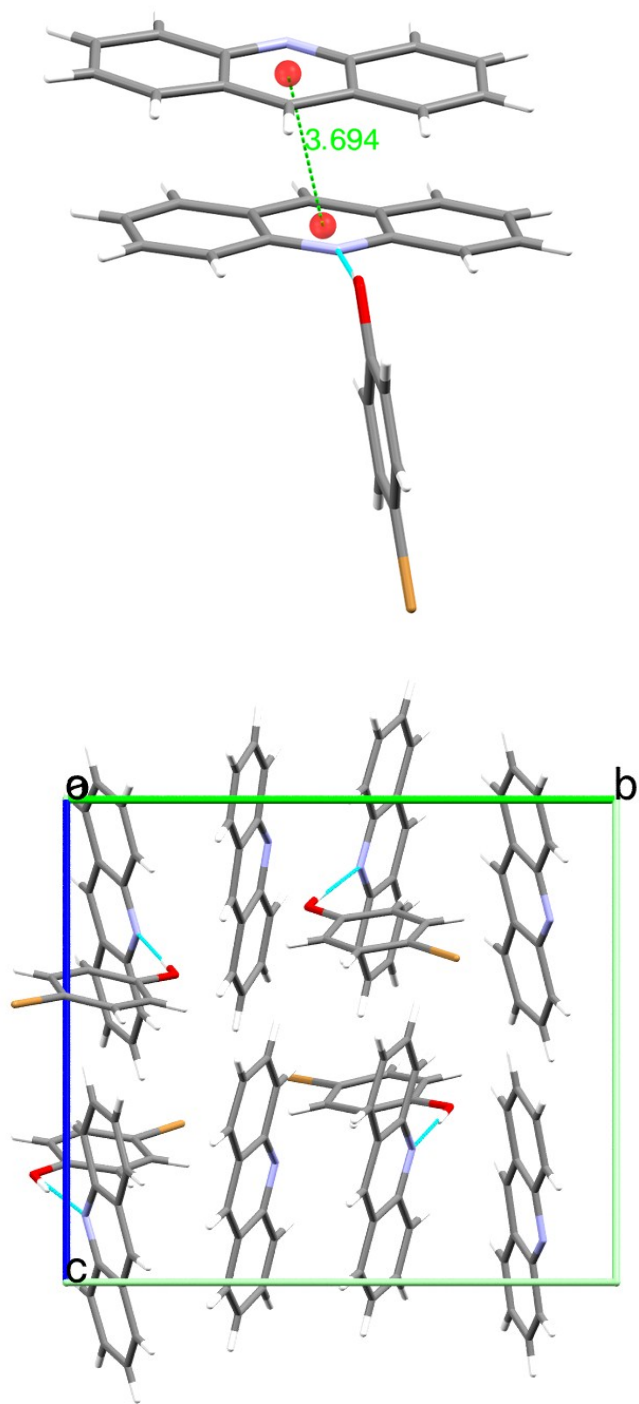


Fig. S8 Crystal structure of $(acr)_2 \cdot (brp)$.

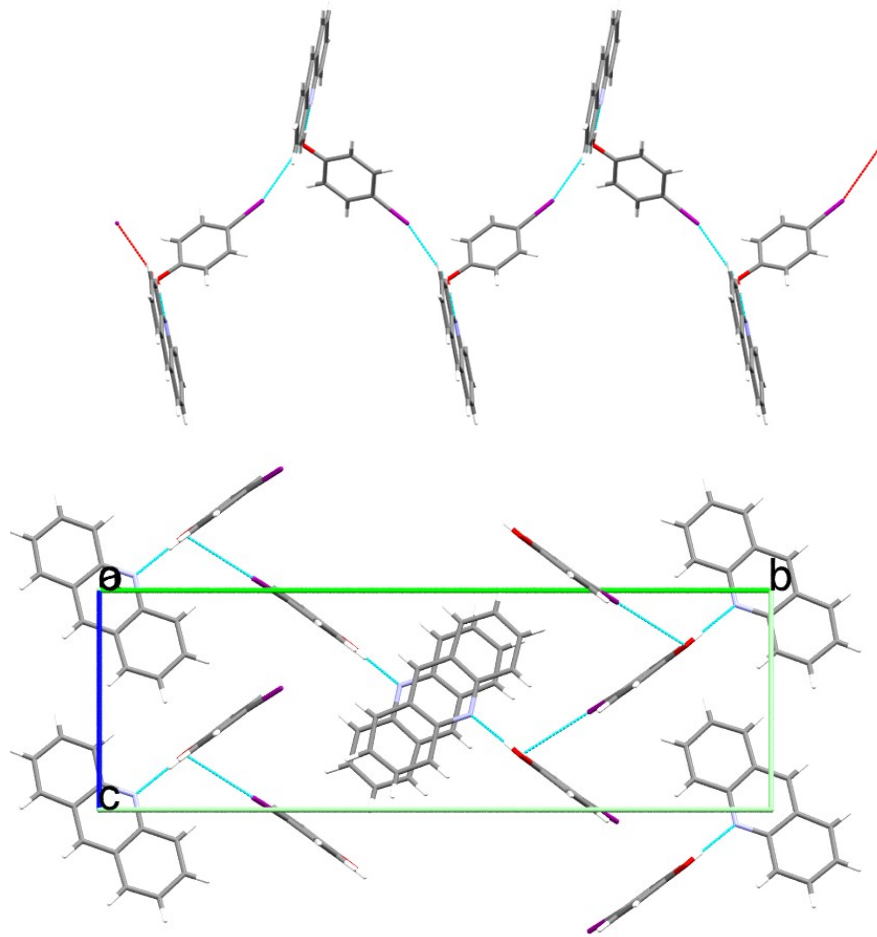


Fig. S9 Crystal structure of (acr)·(ip).

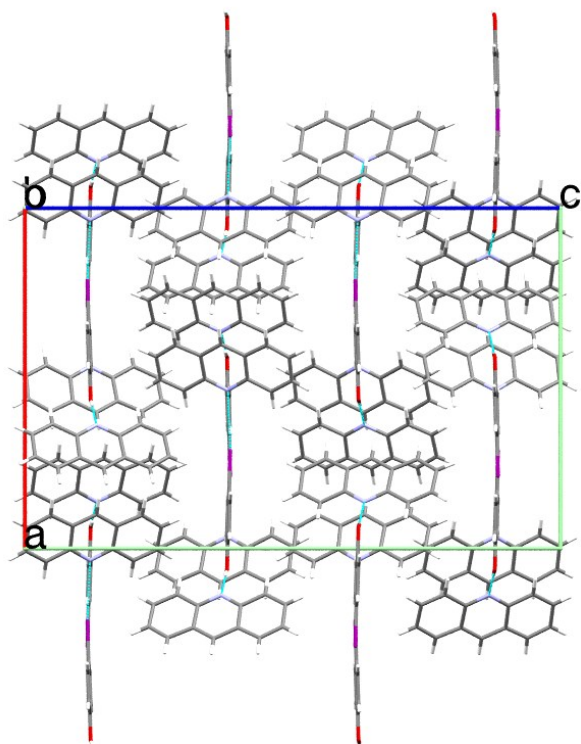
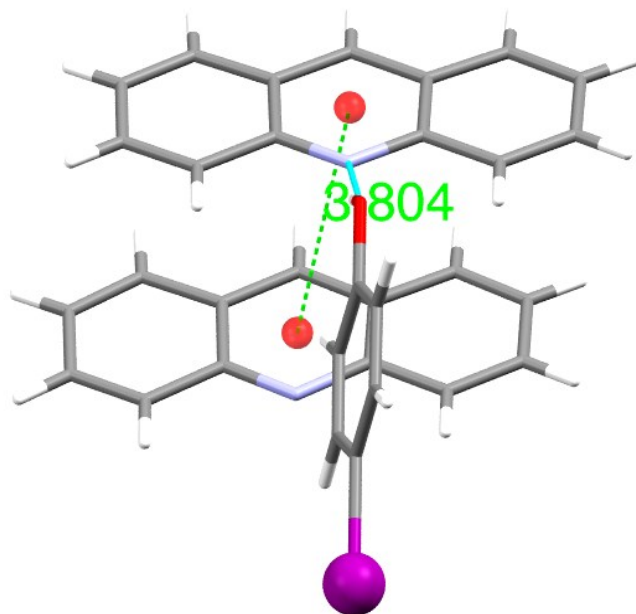


Fig. S10 Crystal structure of $(acr)_2(ip)$.

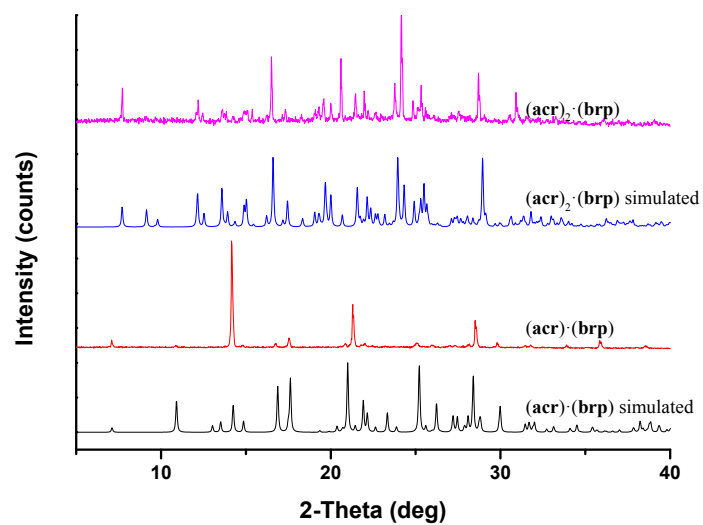


Fig. S11 PXR D patterns of cocrystals $(acr) \cdot (brp)$ and $(acr)_2 \cdot (brp)$.

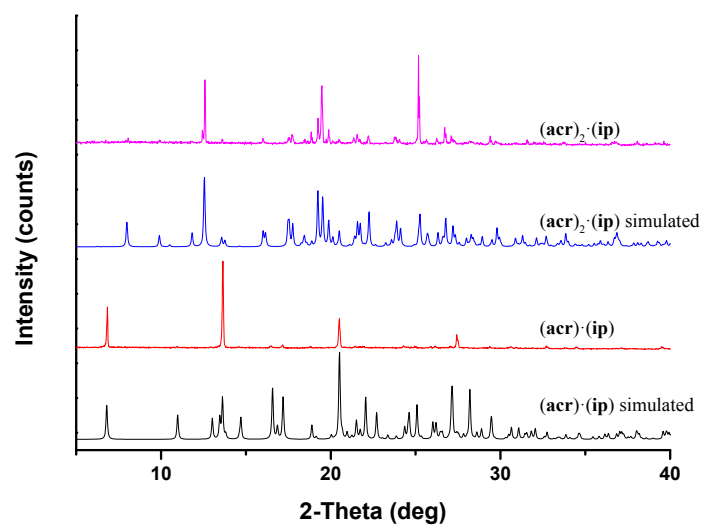


Fig. S12 PXR D patterns of cocrystals $(acr) \cdot (ip)$ and $(acr)_2 \cdot (ip)$.

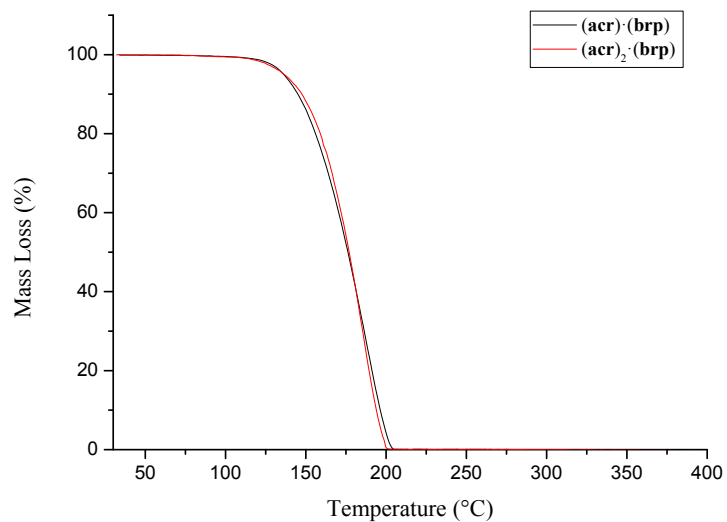


Fig. S13 TGA thermograms of cocrystals **(acr)·(brp)** and **(acr)₂·(brp)**.

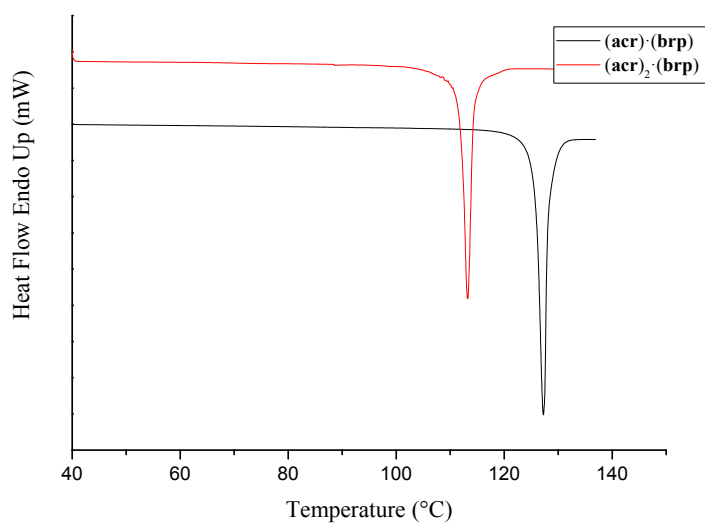


Fig. S14 DSC thermograms of cocrystals **(acr)·(brp)** and **(acr)₂·(brp)**.

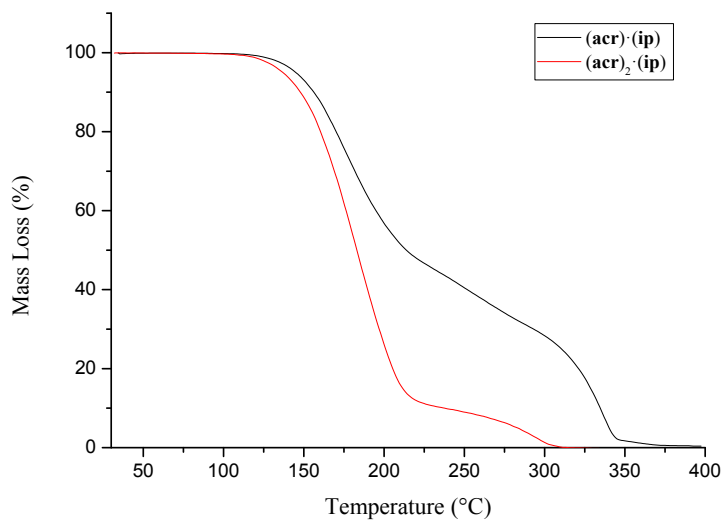


Fig. S15 TGA thermograms of cocrystals (acr)·(ip) and (acr)₂·(ip).

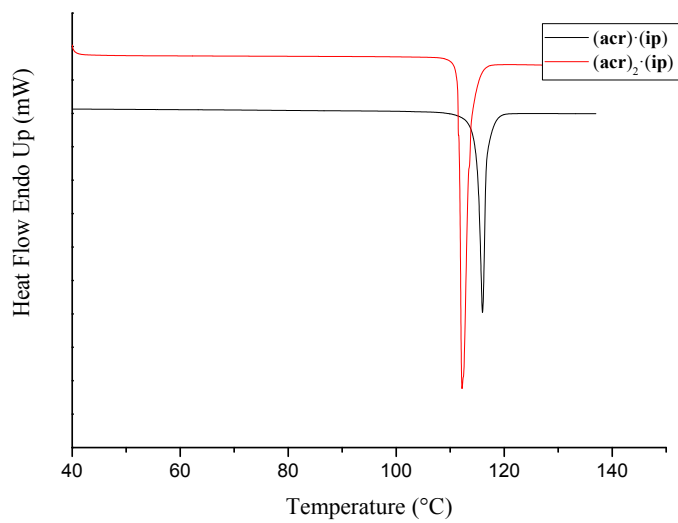


Fig. S16 DSC thermograms of cocrystals (acr)·(ip) and (acr)₂·(ip).

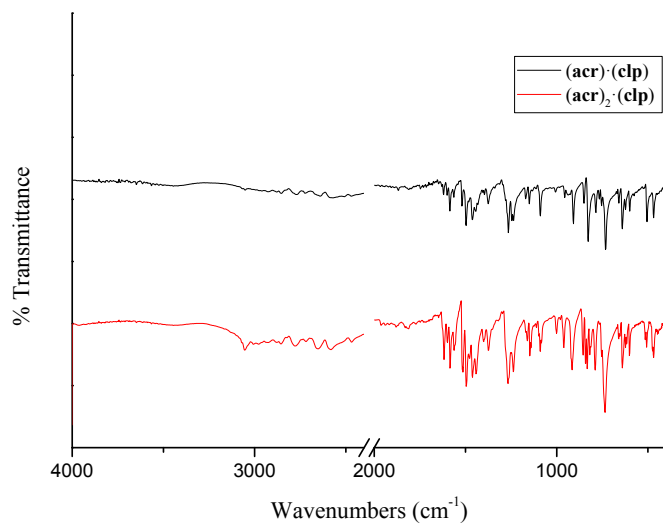


Fig. S17 FT-IR spectra of cococrystals **(acr)·(clp)** and **(acr)₂·(clp)**.

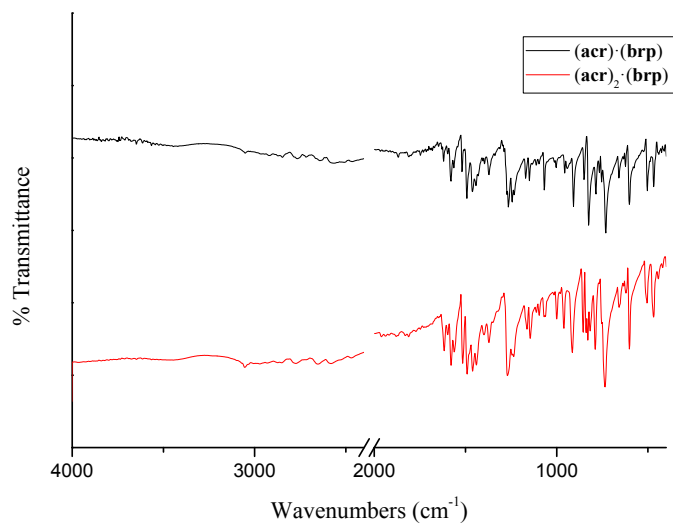


Fig. S18 FT-IR spectra of cococrystals **(acr)·(brp)** and **(acr)₂·(brp)**.

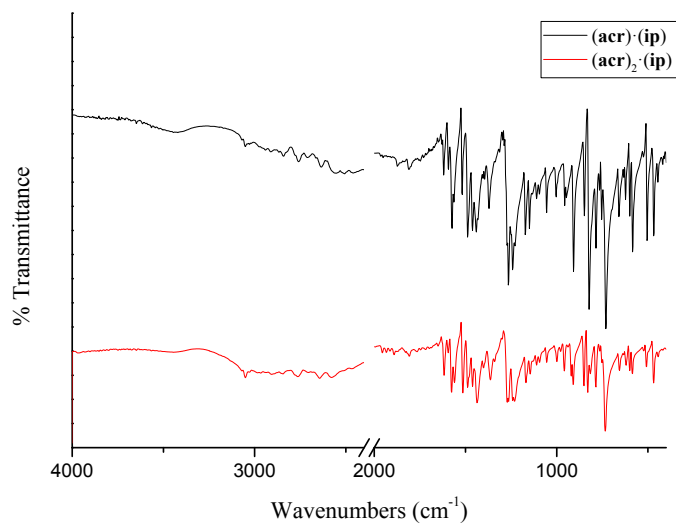


Fig. S19 FT-IR spectra of cocrystals (acr)·(ip) and (acr)₂·(ip).

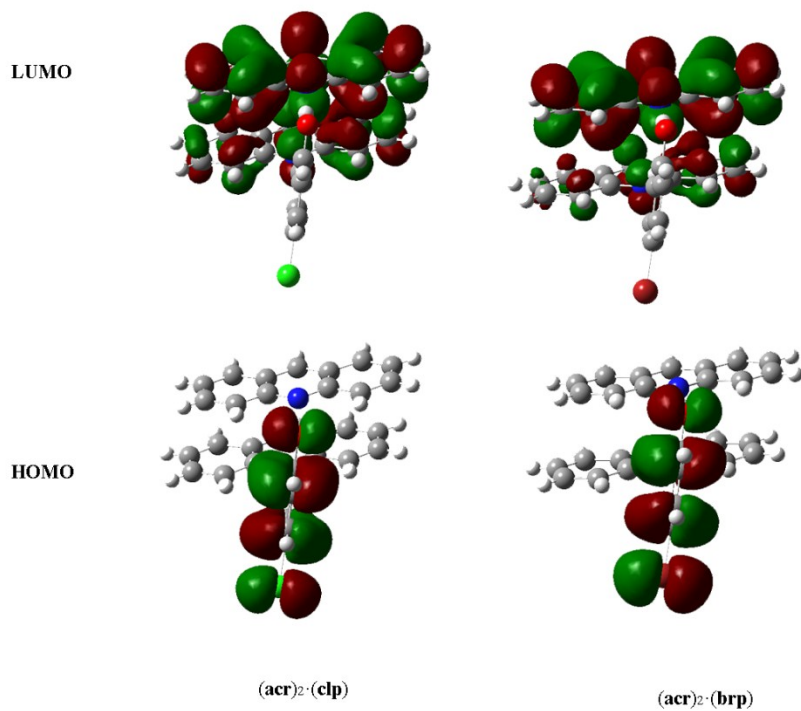


Fig. S20 Frontier molecular orbitals of acr and (acr)₂·(ip).

Table S1 Crystallographic Data for cocrystals.

	(acr)·(clp)	(acr) ₂ ·(clp)	(acr)·(brp)	(acr) ₂ ·(brp)	(acr)·(ip)	(acr) ₂ ·(ip)
Formula	C ₁₉ H ₁₄ ClNO	C ₃₂ H ₂₃ ClN ₂ O	C ₁₉ H ₁₄ BrNO	C ₃₂ H ₂₃ BrN ₂ O	C ₁₉ H ₁₄ INO	C ₃₂ H ₂₃ IN ₂ O
Mr.	307.76	486.97	352.21	531.42	399.21	578.42
Crystal system	Monoclinic	Monoclinic	Monoclinic	Monoclinic	Monoclinic	Orthorhombic
Space group	<i>P</i> 2 ₁ / <i>c</i>	<i>P</i> 2 ₁	<i>P</i> 2 ₁ / <i>c</i>	<i>P</i> 2 ₁	<i>P</i> 2 ₁ / <i>c</i>	<i>Pbca</i>
Temperature (K)	100(2)	170(2)	100(2)	170(2)	100(2)	170(2)
<i>a</i> (Å)	7.0958(5)	12.8719(4)	7.1573(4)	13.0192(2)	7.3010(3)	17.8528(6)
<i>b</i> (Å)	24.4284(17)	14.5519(4)	24.8433(14)	14.6232(3)	25.9817(10)	10.1405(4)
<i>c</i> (Å)	9.0306(7)	14.2914(4)	9.0381(6)	14.2369(2)	9.1022(4)	28.1824(10)
α (°)	90	90	90	90	90	90
β (°)	108.453(3)	115.4000(10)	108.491(3)	115.2880(10)	111.488(2)	90
γ (°)	90	90	90	90	90	90
Cell volume (Å ³)	1484.87(19)	2418.17(12)	1524.11(16)	2450.72(7)	1606.61(11)	5102.0(3)
Calc. density (g/cm ³)	1.377	1.338	1.535	1.440	1.994	1.506
<i>Z</i>	4	4	4	4	4	8
<i>Z'</i>	1	2	1	2	1	1
$\square\square$	0.71073	0.71073	0.71073	0.71073	0.71073	0.71073
<i>S</i>	1.025	1.009	1.003	0.948	1.025	1.010
<i>R</i> ₁	0.031	0.041	0.032	0.032	0.028	0.028
<i>R</i> _{int}	0.021	0.024	0.046	0.046	0.031	0.052
w <i>R</i> ₂	0.084	0.105	0.083	0.083	0.055	0.063

^a*Z* represents the number of cocrystal formula in a unit cell

Table S2 B3LYP/6-31G HOMO and LUMO energies (in eV) at the ground state

	acr	(acr) ₂ ·(clp)	(acr) ₂ ·(brp)	(acr) ₂ ·(ip)
HOMO	-1.85	-2.20	-2.20	-2.28
LUMO	-5.49	-5.33	-5.25	-5.28
ΔE	3.64	3.13	3.05	3.00

